SCIENCE CHINA
Chemistry

•ARTICLES•
SPECIAL ISSUE: Dedicated to the 100th Anniversary of Nankai University

May 2019 Vol.62 No.5: 609–615
https://doi.org/10.1007/s11426-018-9394-1

Freestanding reduced graphene oxide/sodium vanadate composite films for flexible aqueous zinc-ion batteries

Fang Wan[1†], Xinyu Wang[1,2†], Songshan Bi[1], Zhiqiang Niu[1*] & Jun Chen[1]

[1]*Key Laboratory of Advanced Energy Materials Chemistry (Ministry of Education), College of Chemistry, Nankai University, Tianjin 300071, China;*
[2]*Institute of Materials and Technology, Dalian Maritime University, Dalian 116026, China*

Received October 30, 2018; accepted November 26, 2018; published online February 22, 2019

With the booming development of portable and wearable electronic devices, flexible energy storage devices have attracted great attention. Among various energy storage devices, aqueous zinc ion batteries (ZIBs) are one of the promising candidates due to their low cost, good safety, high energy and power densities. However, the conventional cathodes of aqueous ZIBs were often prepared by mixing active materials with binders and conductive additives and then coating them onto current collectors. The resultant cathodes often suffer from unsatisfied flexibility. Herein, we fabricated freestanding reduced graphene oxide/NaV_3O_8•$1.5H_2O$ (RGO/NVO) composite films with interlinked multilayered architecture by a vacuum filtrating process. Such composite films exhibit excellent mechanical property and high electronic conductivity. Owing to unique architecture, they display a high capacity of 410 mA h g^{-1} and excellent cycling performance up to 2000 cycles with a high capacity retention of 94%. Moreover, RGO/NVO composite films can directly serve as the cathodes of flexible aqueous ZIBs. As a proof of concept, flexible ZIBs were assembled based on the composite films. Impressively, they exhibit stable performance at different bending states, demonstrating great potential application in flexible energy storage devices.

zinc-ion battery, graphene, NaV_3O_8•$1.5H_2O$, composite film, flexibility

Citation: Wan F, Wang X, Bi S, Niu Z, Chen J. Freestanding reduced graphene oxide/sodium vanadate composite films for flexible aqueous zinc-ion batteries. *Sci China Chem*, 2019, 62: 609–615, https://doi.org/10.1007/s11426-018-9394-1

1 Introduction

The booming development of portable and wearable electronic devices has triggered the urgent demand for flexible energy storage systems [1–4]. Recently, significant efforts have been implemented to develop flexible energy storage devices, such as supercapacitors and lithium-ion batteries [5–8]. Supercapacitors have high power density and long cycle life, but suffer from low energy density. In contrast, lithium-ion batteries based on organic electrolytes show high energy density, but limited power density and unsatisfied cycle performance. In this regard, aqueous batteries are considered because they not only deliver the intrinsical energy density of batteries, but also display improved power density because of the high ionic conductivity of aqueous electrolyte, thus bridging the gap between supercapacitors and traditional lithium-ion batteries [9,10]. Among various aqueous batteries, aqueous zinc-ion batteries (ZIBs) are attracting more attention due to their impressive advantages, such as low cost, good safety, low redox potential (−0.76 V vs. standard hydrogen electrode) and high theoretical capacity of Zn (820 mA h g^{-1} and 5855 mA h cm^{-3}) [11–17]. Thus, flexible aqueous ZIBs will be one of promising energy storage devices for portable and wearable electronics.

Successful assembly of flexible aqueous ZIBs mainly de-

†The authors contributed equally to this work.
*Corresponding author (email: zqniu@nankai.edu.cn)

pends on the design of cathode materials as well as configurations. Recently, the cathode materials of aqueous ZIBs mainly focused on MnO_2 [18–20], Prussian blue analogues [21–23], organic compounds [24–27] and vanadium-based materials [28–34]. However, the electrodes based on these cathode materials were often prepared by mixing them with binders and conductive additives and then coating the slurry onto current collectors. The resultant electrodes often suffer from the cracking and exfoliation of active material during bending process and thus exhibit unsatisfied flexibility. Owing to the unique two-dimensional structure, graphene is an ideal building block to construct macroscopic graphene and graphene-based composite films with high conductivity and flexibility [35–39]. In addition, NaV_3O_8•$1.5H_2O$ (NVO) nanobelts have been confirmed to be one of the promising cathode materials of aqueous ZIBs in our previous report [34]. However, the capacity of NVO is far from the theoretical value (486 mA h g^{-1} based on V^{5+}/V^{3+}) due to the low conductivity of NVO. If NVO nanobelts are introduced into graphene-based films, high conductive and flexible composite film cathodes of aqueous ZIB would be obtained.

Herein, we fabricated freestanding reduced graphene oxide/NVO (RGO/NVO) nanocomposite films by a vacuum filtration strategy. The RGO/NVO composite films possess interlinked multilayered architecture, in which the NVO nanobelts were homogeneously distributed and tightly contacted with RGO nanosheets. Furthermore, the freestanding RGO/NVO cathode films display excellent mechanical property and high conductivity. As a result, the RGO/NVO composite films can directly serve as the electrodes of flexible ZIBs. The resultant flexible ZIBs show stable electrochemical performance at different bending states.

2 Experimental

2.1 Preparation of NVO/RGO composite films

NVO nanobelts were synthetized as our previously reported method [34]. Typically, 1 g of commercial V_2O_5 powder was added into 15 mL of 2 M NaCl aqueous solution. After stirring for 96 h at 30 °C, NVO nanobelts were formed. And then, the suspension was washed by deionized water for several times, and then freeze-dried.

Graphene oxide (GO) suspension was prepared via a modified Hummers' method [40]. To reduce GO, hydrazine (1.5 mL) and NH_3•H_2O (2.5 mL) were added into GO suspension (100 mL, 0.1 mg mL^{-1}), then stirring for 3 h at 95 °C. Subsequently, the RGO suspension was washed to neutral by a dialysis method. The concentration of resultant RGO suspension is 0.07 mg mL^{-1} (Figure S1, Supporting Information online).

To prepare RGO/NVO composite films with different NVO contents, 15 mg NVO was added into RGO suspension with various volumes, followed by 1 h ultrasonication. The mass ratio of NVO and RGO was controlled at 8:2, 7:3, 6:4, and 5:5 (denoted as RGO/NVO-80%, RGO/NVO-70%, RGO/NVO-60%, RGO/NVO-50%). The RGO/NVO composite films were obtained by vacuum filtrating the RGO/NVO suspension, and then freeze-drying. The mass loading of NVO in RGO/NVO films was ~1.2 mg cm^{-2}.

2.2 Assembly of Zn//RGO/NVO batteries

CR2032 coin cells were assembled by a traditional method using RGO/NVO composite films, filter papers (thickness: 150 μm, diameter: 16 mm), and Zn foils (thickness: 30 μm, diameter: 10 mm) as positive electrodes, separators, and negative electrodes, respectively. Soft-packaged batteries were assembled by sandwiching separators between the RGO/NVO composite films and Zn foils, and then injecting electrolyte and being sealed by Al-plastic films. The electrolyte for coin cells and soft-packaged batteries was 1 M $ZnSO_4$/1 M Na_2SO_4 aqueous solution.

2.3 Characterization

The morphology and microstructure of NVO nanobelts and RGO/NVO composite films were characterized by scanning electron microscopy (SEM; JEOL JSM-7500F, Japan) and transmission electron microscopy (TEM; JEOL-2100F, Japan) with energy dispersive spectroscopy (EDS) for elemental analysis. X-ray diffraction (XRD) measurements were implemented on Rigaku Ultima IV (Japan) with Cu Kα radiation to characterize the crystal structure of NVO and RGO/NVO composite films. The tensile tests of the pure RGO film and RGO/NVO composite films were carried out on dynamic mechanical analyzer (DMA; Q800, TA Instruments, USA). The sheet resistances of the pure RGO and RGO/NVO composite films were tested by Keithley 2400 Source Meter (USA). Cyclic voltammetry (CV) was measured using an electrochemical workstation (CHI 660E) with a voltage window between 0.3 and 1.3 V at different scan rates from 0.1 to 1.0 mV s^{-1}. Galvanostatic charge/discharge tests were implemented on a battery test system (LAND CT2001A, China) with a voltage window between 0.3 and 1.3 V. For coin cells, the current densities for rate test are 0.1, 0.2, 0.5, 1, 2, 3, 4 and 5 A g^{-1}, and for cycling measurement is 5 A g^{-1}. For the soft-packaged ZIBs, the applied current density for electrochemical measurement is 1 A g^{-1}.

3 Results and discussion

Since the as-prepared NVO nanobelts have high aspect ratio (Figure S2) and RGO sheets have the surfactant effect due to the hydrophobic basal plane and hydrophilic edges [41],

NVO nanobelts can homogeneously distribute in RGO suspension to form RGO/NVO suspension. Freestanding RGO/NVO composite films will be easily obtained by a simple vacuum filtration process, which is a flow-directed assembly using shearing field-assisted alignment of RGO/NVO suspension [42]. The mass loadings and thicknesses of the freestanding RGO/NVO composite films can be controlled by the mass of NVO and the volume of RGO suspension. The resultant RGO/NVO composite films are interlinked multilayered architecture (Figure 1(c)), where NVO nanobelts contact with RGO sheets intimately, guaranteeing the high flexibility of RGO/NVO composite films. Even the mass content of NVO is up to 70%, the resultant freestanding RGO/NVO films are still flexible as well as mechanically stable without obvious crack during bending (Figure 1(a)). The thickness of RGO/NVO-70% composite film is ~25 μm, as shown in the cross-sectional SEM image (Figure 1(b)). SEM images also display the homogeneous dispersion of NVO nanobelts and RGO sheets throughout the entire composite films (Figure 1(c, d)). Even the content of NVO in RGO/NVO composite film is changed, the NVO nanobelts can still be homogeneously distributed in RGO network (Figure S3). In addition, the morphology of NVO nanobelts in RGO/NVO composite films is similar to the primary state, indicating the preparation process have no obvious influence on the NVO (Figure 1(e, f)). In such RGO/NVO composite films, the RGO sheets are tightly attached to the surface of NVO nanobelts, and in turn, the nanobelts sandwiched between the RGO sheets can prevent their restacking and aggregating. This architecture affords a good deal of pores and channels, which allows more efficient contact between electrolyte and cathode materials, thus promoting ion transport throughout the RGO/NVO composite films.

The XRD patterns of RGO/NVO composite films are well indexed to NVO with a $P2_1/m$ space group (JCPDS: 16-0601) except the broad peak at ~24° with a relatively low intensity, which is ascribed to the (002) plane of RGO (Figure 2(a)). This indicates that the introduction of RGO has no obvious effect on the crystalline of NVO. To serve as the flexible electrodes, superior mechanical property, high electronic conductivity, and stable sheet resistance of RGO/NVO composite films are required. In our case, the RGO/NVO composite film can endure a tensile strength of 11 MPa and the fracture strain of the RGO/NVO composite film reaches to 1.6% even the NVO mass content is up to 80% (Figure 2(b)). This result originates from the interlinkage between RGO sheets and NVO nanobelts in RGO/NVO composite films. Such unique architecture also endows the RGO/NVO composite films with high electronic conductivity. The sheet resistance of the RGO/NVO composite films with 80% NVO (mass content) is only 55 Ω (Figure 2(c)). Furthermore, it is noted that the sheet resistances of these composite films remain unchanged even under different bending states (Figure 2(d)). As a result, the RGO/NVO composite films could directly serve as the freestanding positive electrodes of flexible ZIBs without the assistance of any current collector and binder.

The electrochemical performance of the RGO/NVO composite films was first investigated in coin cells. With the increase of NVO content, the capacity (based on the mass of composite films) of RGO/NVO composite films enhances when NVO content is less than 70% (Figure S4). The improvement of the capacity could be explained by the fact that there are more available NVO in the composite films. However, the capacity decreases with the further increase of NVO content, because a portion of the RGO conductive

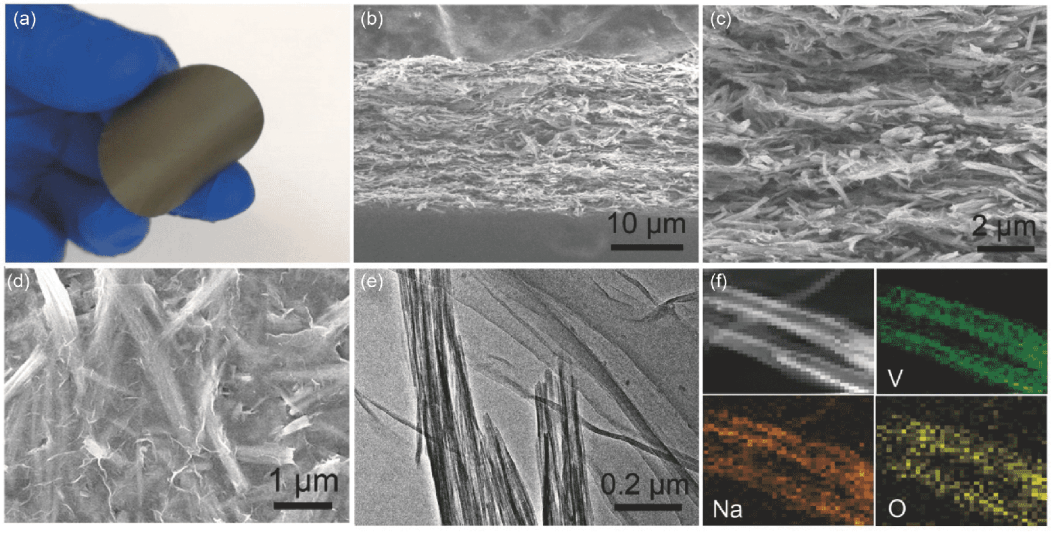

Figure 1 (a) Optical image, (b, c) cross-sectional SEM images, (d) top-view SEM image, and (e) TEM image of RGO/NVO-70% composite film. (f) TEM elemental mapping images of NVO nanobelts (color online).

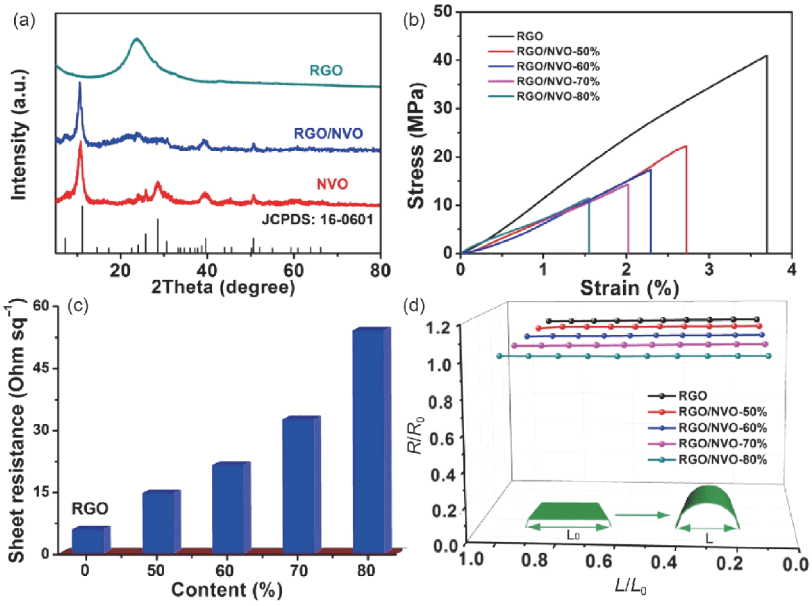

Figure 2 (a) XRD patterns of RGO film, NVO nanobelts, and RGO/NVO composite film. (b) Stress-strain curves of RGO and RGO/NVO composite films. (c) Sheet resistances of RGO and RGO/NVO composite films. (d) The normalized sheet resistances of RGO and RGO/NVO composite films at different bending states, where R_0 and L_0 are the initial sheet resistance and length of RGO or RGO/NVO composite films, respectively; R and L are the sheet resistance and distance between two ends of these films under different bending states, respectively. Inset shows the schematic diagram of bending (color online).

network is interrupted, thus impeding the effective transport of electrons in corresponding electrode. As a result, the proportion of NVO in RGO/NVO composite film is controlled at 70% in the following section.

Figure 3(a) displays the galvanostatic charge/discharge profiles of RGO/NVO-70% composite films at different current densities from 0.1 to 5 A g^{-1}. Owing to the unique interlinked multilayered architecture and a good deal of pores, RGO/NVO composite films possess high electronic conductivity and abundant ion transport channels. As a result, a high capacity of 410 mA h g^{-1} (based on the mass of NVO) is achieved at 0.1 A g^{-1} in RGO/NVO composite films-based batteries, which is higher than that (380 mA h g^{-1}) of conventional NVO-based batteries in our previous report [34]. The capacity can still remain at 150 mA h g^{-1} even at a high current density of 5 A g^{-1}, which is 36.6% of that at 0.1 A g^{-1}. In addition, there are two pairs of obvious plateaus located at around 0.59/0.76 and 0.84/1.00 V, which can be ascribed to the redox of NVO during charge/discharge process. Moreover, these plateaus in charge/discharge curves can still be clearly distinguished even at the high current density of 5 A g^{-1}. These results clearly demonstrate that the RGO/NVO-70% composite film-based ZIBs deliver superior rate capability. In addition to the rate capability, cycling performance is also an important factor for the application of aqueous ZIBs. Figure 3(e) shows the cycling performance of RGO/NVO composite films at a current density of 5 A g^{-1}. Even after 2000 cycles, a high capacity retention of 94% is achieved, which is much better than conventional NVO-based batteries (a capacity retention of 82% after 1000 cycles at 4 A g^{-1}) [34]. Moreover, the coulombic efficiency is near 100% except the first cycle.

Figure 3(b) exhibits the cyclic voltammetry (CV) curves of RGO/NVO composite electrode from 0.1 to 1.0 mV s^{-1} with the voltage window between 0.3 and 1.3 V. Even the scan rate increases to 1.0 mV s^{-1}, two pairs of redox peaks are still obvious and show slight shift, indicating that the RGO/NVO composite electrode possesses fast kinetics. In addition, the relationship between peak currents (i) and scan rates (v) can be described as the following equation [43,44]:

$$i = av^b \quad (1)$$

The equation can also be written as:

$$\log i = b\log v + \log a \quad (2)$$

where a and b are adjustable parameters. b is determined by the slope of log$i$-log$v$ curve, which often changes from 0.5 to 1. When b is 0.5, the charge/discharge process is dominated by ionic diffusion. However, if b is 1, the charge/discharge process is controlled by surface controlling. By fitting the log$i$-log$v$ curve, the b values of peak 1, 2, 3 and 4 correspond to 0.60, 0.76, 0.59 and 0.80, respectively (Figure 3(c)), demonstrating that the electrochemical process of Zn//RGO/NVO batteries is dominated by ionic diffusion and surface controlling simultaneously. This leads to a fast Zn^{2+} diffusion kinetics, enabling the high rate capability. Furthermore, the surface controlled contribution can be calculated through the following equation [45,46]:

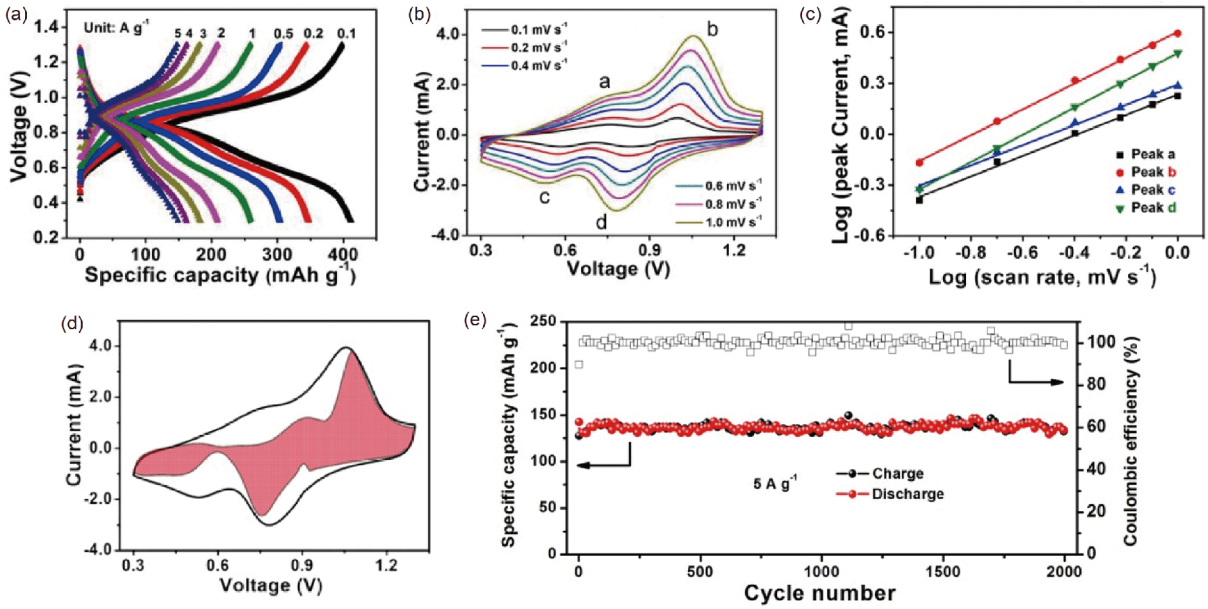

Figure 3 (a) Charge/discharge curves of RGO/NVO-70% composite film-based ZIBs at different current densities; (b) CV curves of RGO/NVO-70% composite film-based ZIBs at different scan rates; (c) the corresponding log(peak current) versus log(scan rate) plots at each redox peak; (d) surface-controlled capacity contributions at 0.1 mV s^{-1}; (e) long cycle life of RGO/NVO-70% composite film-based ZIBs at 5 A g^{-1} (color online).

$$i = k_1 v + k_2 v^{1/2} \quad (3)$$

which can be reformulated as:

$$i / v^{1/2} = k_1 v^{1/2} + k_2 \quad (4)$$

where i, $k_1 v$, and $k_2 v^{1/2}$ represent the current response, surface controlled contribution, and ionic diffusion contribution, respectively. Since k_1 can be obtained by fitting the $i/v^{1/2}$ and $v^{1/2}$ plots, the surface controlled contribution is calculated to be 41.3% at the scan rate of 0.1 mV s^{-1} (Figure 3(d)). With the increase of scan rates, the percentage of surface controlled contribution increases to 46.5%, 55.6%, 60.9%, 64.4% and 68.2% at the scan rates of 0.2, 0.3, 0.4, 0.5 and 1 mV s^{-1}, respectively (Figure S5), revealing that the Zn// RGO/NVO batteries have fast charge transfer kinetics.

The excellent mechanical property and high electronic conductivity of RGO/NVO composite films endow them with the ability to serve as the cathodes of flexible ZIBs directly. As a proof of concept, we fabricated flexible soft-packaged ZIBs based on RGO/NVO composite films, as shown in Figure 4(a). There are still two obvious discharge

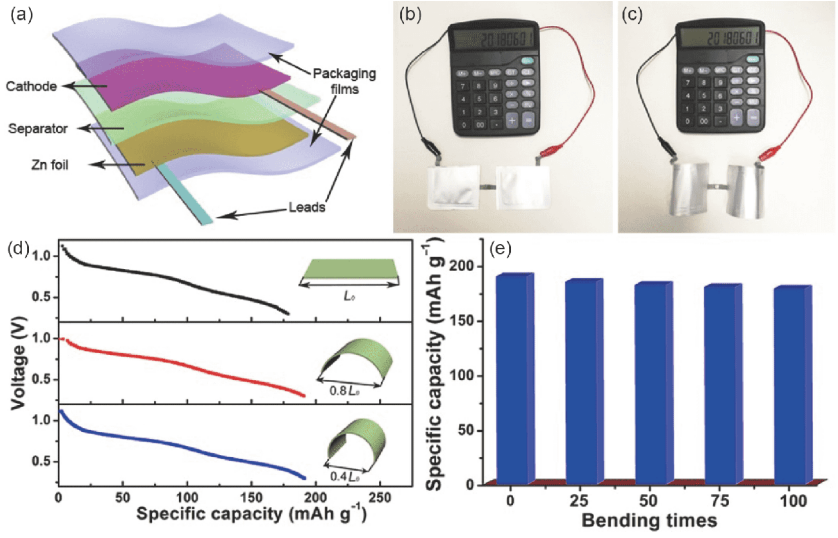

Figure 4 (a) Schematic diagram of flexible soft-packaged ZIBs. Optical images of a calculator powered by two soft-packaged ZIBs in series under (b) flat state and (c) bending state. (d) Discharge curves of the flexible soft-packaged ZIBs at 1 A g^{-1} under different bending states. Insets show the schematic diagrams of different bending states. (e) The relationship between capacity and bending times (the soft-packaged ZIBs were bent to $0.4L_0$, where L_0 is the initial length of soft-packaged ZIBs) (color online).

plateaus in the discharge curves of the as-prepared soft-packaged ZIBs, which are similar to those of coin cells (Figure 4(d)). It indicates that the soft-packaged configuration nearly has no influence on the reaction mechanism of Zn//RGO/NVO systems. To illustrate the flexibility of the soft-packaged ZIBs, they were bent to different states (insets of Figure 4(d)). Impressively, the discharge plateau is almost unchanged and the capacity is not obviously degraded (Figure 4(d)). In addition, an important factor for the application of flexible devices is to achieve stable electrochemical performance after repeated bending. The resultant soft-packaged ZIBs can endure 100 bending cycles without obvious capacity decaying (Figure 4(e)), showing their application potential as flexible energy storage devices. Furthermore, the flexibility of the resultant soft-packaged ZIBs was also demonstrated via a simple visual cue (Figure 4(b, c)). Two soft-packaged Zn//RGO/NVO batteries in series can power a calculator. The calculator could still work well when the soft-packaged batteries were subjected to bending, indicating the flexibility of the soft-packaged Zn//RGO/NVO batteries.

4 Conclusions

In summary, freestanding RGO/NVO composite films were prepared via a vacuum filtration strategy. The resultant RGO/NVO composite films possess interlinked multilayered architecture, where NVO nanobelts are homogeneously distributed in RGO network and contact with RGO intimately. Since such composite films display excellent mechanical property and high electronic conductivity, they can be used as the cathodes of aqueous ZIBs directly without any current collector and binder. The unique architecture of RGO/NVO composite films endows them with excellent electrochemical performance in terms of a high capacity of 410 mA h g^{-1}, superior cycling performance with a high capacity retention of 94% after 2000 cycles at 5 A g^{-1}. Furthermore, the freestanding RGO/NVO composite films can act as the electrodes of flexible ZIBs. As a proof of concept, the soft-packaged aqueous ZIBs based on them deliver stable electrochemical performance at different bending states, even after 100 repeated bending cycles.

Acknowledgements This work was supported by the National Natural Science Foundation of China (21573116, 51822205, 21875121, 51602218), Ministry of Science and Technology of China (2017YFA0206701), Ministry of Education of China (B12015), Tianjin Basic and High-Tech Development (16PTSYJC00030), the Fundamental Research Funds for the Central Universities and the Young Thousand Talents Program.

Conflict of interest The authors declare that they have no conflict of interest.

Supporting information The supporting information is available online at http://chem.scichina.com and http://link.springer.com/journal/11426. The supporting materials are published as submitted, without typesetting or editing. The responsibility for scientific accuracy and content remains entirely with the authors.

1 Zeng Y, Zhang X, Meng Y, Yu M, Yi J, Wu Y, Lu X, Tong Y. *Adv Mater*, 2017, 29: 1700274
2 Li H, Han C, Huang Y, Huang Y, Zhu M, Pei Z, Xue Q, Wang Z, Liu Z, Tang Z, Wang Y, Kang F, Li B, Zhi C. *Energy Environ Sci*, 2018, 11: 941–951
3 Liu L, Niu Z, Chen J. *Chem Soc Rev*, 2016, 45: 4340–4363
4 Niu Z, Liu L, Zhang L, Zhou W, Chen X, Xie S. *Adv Energy Mater*, 2015, 5: 1500677
5 Chen C, Cao J, Lu Q, Wang X, Song L, Niu Z, Chen J. *Adv Funct Mater*, 2016, 27: 1604639
6 Amin K, Meng Q, Ahmad A, Cheng M, Zhang M, Mao L, Lu K, Wei Z. *Adv Mater*, 2018, 30: 1703868
7 Li S, Meng X, Yi Q, Alonso JA, Fernández-Díaz MT, Sun C, Wang ZL. *Nano Energy*, 2018, 52: 510–516
8 Chen C, Cao J, Wang X, Lu Q, Han M, Wang Q, Dai H, Niu Z, Chen J, Xie S. *Nano Energy*, 2017, 42: 187–194
9 Kim H, Hong J, Park KY, Kim H, Kim SW, Kang K. *Chem Rev*, 2014, 114: 11788–11827
10 Yamada Y, Usui K, Sodeyama K, Ko S, Tateyama Y, Yamada A. *Nat Energy*, 2016, 1: 16129
11 Kundu D, Adams BD, Duffort V, Vajargah SH, Nazar LF. *Nat Energy*, 2016, 1: 16119
12 Pan H, Shao Y, Yan P, Cheng Y, Han KS, Nie Z, Wang C, Yang J, Li X, Bhattacharya P, Mueller KT, Liu J. *Nat Energy*, 2016, 1: 16039
13 Zhang N, Dong Y, Jia M, Bian X, Wang Y, Qiu M, Xu J, Liu Y, Jiao L, Cheng F. *ACS Energy Lett*, 2018, 3: 1366–1372
14 Yang Y, Tang Y, Fang G, Shan L, Guo J, Zhang W, Wang C, Wang L, Zhou J, Liang S. *Energy Environ Sci*, 2018, 11: 3157–3162
15 Li G, Yang Z, Jiang Y, Jin C, Huang W, Ding X, Huang Y. *Nano Energy*, 2016, 25: 211–217
16 Fang G, Zhou J, Pan A, Liang S. *ACS Energy Lett*, 2018, 3: 2480–2501
17 Song M, Tan H, Chao D, Fan HJ. *Adv Funct Mater*, 2018, 28: 1802564
18 Xu C, Li B, Du H, Kang F. *Angew Chem Int Ed*, 2012, 51: 933–935
19 Sun W, Wang F, Hou S, Yang C, Fan X, Ma Z, Gao T, Han F, Hu R, Zhu M, Wang C. *J Am Chem Soc*, 2017, 139: 9775–9778
20 Zhang N, Cheng F, Liu J, Wang L, Long X, Liu X, Li F, Chen J. *Nat Commun*, 2017, 8: 405
21 Zhang L, Chen L, Zhou X, Liu Z. *Adv Energy Mater*, 2015, 5: 1400930
22 Trócoli R, La Mantia F. *ChemSusChem*, 2015, 8: 481–485
23 Zhang L, Chen L, Zhou X, Liu Z. *Sci Rep*, 2015, 5: 18263
24 Wan F, Zhang L, Wang X, Bi S, Niu Z, Chen J. *Adv Funct Mater*, 2018, 28: 1804975
25 Guo Z, Ma Y, Dong X, Huang J, Wang Y, Xia Y. *Angew Chem Int Ed*, 2018, 57: 11737–11741
26 Kundu D, Oberholzer P, Glaros C, Bouzid A, Tervoort E, Pasquarello A, Niederberger M. *Chem Mater*, 2018, 30: 3874–3881
27 Zhao Q, Huang W, Luo Z, Liu L, Lu Y, Li Y, Li L, Hu J, Ma H, Chen J. *Sci Adv*, 2018, 4: eaao1761
28 Chao D, Zhu CR, Song M, Liang P, Zhang X, Tiep NH, Zhao H, Wang J, Wang R, Zhang H, Fan HJ. *Adv Mater*, 2018, 30: 1803181
29 Yan M, He P, Chen Y, Wang S, Wei Q, Zhao K, Xu X, An Q, Shuang Y, Shao Y, Mueller KT, Mai L, Liu J, Yang J. *Adv Mater*, 2018, 30: 1703725
30 Alfaruqi MH, Mathew V, Song J, Kim S, Islam S, Pham DT, Jo J, Kim S, Baboo JP, Xiu Z, Lee KS, Sun YK, Kim J. *Chem Mater*, 2017, 29: 1684–1694
31 Dai X, Wan F, Zhang L, Cao H, Niu Z. *Energy Storage Mater*, 2018, doi: 10.1016/j.ensm.2018.07.022
32 Hu P, Zhu T, Wang X, Wei X, Yan M, Li J, Luo W, Yang W, Zhang

W, Zhou L, Zhou Z, Mai L. *Nano Lett*, 2018, 18: 1758–1763
33 Soundharrajan V, Sambandam B, Kim S, Alfaruqi MH, Putro DY, Jo J, Kim S, Mathew V, Sun YK, Kim J. *Nano Lett*, 2018, 18: 2402–2410
34 Wan F, Zhang L, Dai X, Wang X, Niu Z, Chen J. *Nat Commun*, 2018, 9: 1656
35 Yang S, Lohe MR, Müllen K, Feng X. *Adv Mater*, 2016, 28: 6213–6221
36 Tang L, Wang Y, Li Y, Feng H, Lu J, Li J. *Adv Funct Mater*, 2009, 19: 2782–2789
37 Cao J, Chen C, Chen K, Lu Q, Wang Q, Zhou P, Liu D, Song L, Niu Z, Chen J. *J Mater Chem A*, 2017, 5: 15008–15016
38 Cheng HM. *Sci China Chem*, 2018, 61: 1475–1476
39 Ma J, Xiang Z, Zhang J. *Sci China Chem*, 2018, 61: 592–597
40 Luo S, Yao M, Lei S, Yan P, Wei X, Wang X, Liu L, Niu Z. *Nanoscale*, 2017, 9: 4646–4651
41 Kim J, Cote LJ, Kim F, Yuan W, Shull KR, Huang J. *J Am Chem Soc*, 2010, 132: 8180–8186
42 Dikin DA, Stankovich S, Zimney EJ, Piner RD, Dommett GHB, Evmenenko G, Nguyen SBT, Ruoff RS. *Nature*, 2007, 448: 457–460
43 Zhang K, Park M, Zhou L, Lee GH, Li W, Kang YM, Chen J. *Adv Funct Mater*, 2016, 26: 6728–6735
44 Chao D, Zhu C, Yang P, Xia X, Liu J, Wang J, Fan X, Savilov SV, Lin J, Fan HJ, Shen ZX. *Nat Commun*, 2016, 7: 12122
45 Chao D, Liang P, Chen Z, Bai L, Shen H, Liu X, Xia X, Zhao Y, Savilov SV, Lin J, Shen ZX. *ACS Nano*, 2016, 10: 10211–10219
46 Xia X, Chao D, Zhang Y, Zhan J, Zhong Y, Wang X, Wang Y, Shen ZX, Tu J, Fan HJ. *Small*, 2016, 12: 3048–3058